^{11}C-PBR28 and ^{18}F-PBR111 Detect White Matter Inflammatory Heterogeneity in Multiple Sclerosis

Gourab Datta[1], Alessandro Colasanti[1,2], Nicola Kalk[1], David Owen[1], Gregory Scott[1], Eugenii A. Rabiner[3], Roger N. Gunn[1,3], Anne Lingford-Hughes[1], Omar Malik[1], Olga Ciccarelli[4], Richard Nicholas[1], Lei Nei[5], Marco Battaglini[6], Nicola D. Stefano[6], and Paul M. Matthews[1]

[1]Division of Brain Sciences, Department of Medicine, Imperial College London, London, United Kingdom; [2]Centre for Affective Disorders, Psychological Medicine, Institute of Psychiatry, Psychology and Neuroscience, King's College London, London, United Kingdom; [3]Imanova Centre for Imaging Sciences, London, United Kingdom; [4]Queen Square Multiple Sclerosis Centre, Institute of Neurology, University College London, London, United Kingdom; [5]Department of Computing, Imperial College London, London, United Kingdom; and [6]Department of Medicine, Surgery and Neurology, University of Siena, Siena, Italy

The objective of this study was to assess microglial activation in lesions and in normal-appearing white matter (NAWM) of multiple sclerosis (MS) patients using PET. **Methods:** Thirty-four MS patients (7 with secondary progressive MS [SPMS], 27 with relapsing remitting MS [RRMS]) and 30 healthy volunteers, genetically stratified for translocator protein (TSPO) binding status, underwent PET scanning with TSPO radioligands (^{11}C-PBR28 or ^{18}F-PBR111). Regional TSPO availability was measured as a distribution volume ratio (DVR) relative to the caudate (a pseudoreference region). White matter lesions (WMLs) were classified as "active" (DVR highest in the lesion), "peripherally active" (perilesional DVR highest), "inactive" (DVR highest in surrounding NAWM), or "undifferentiated" (similar DVR across lesion, perilesional and NAWM volumes). **Results:** The mean DVR in NAWM of patients was greater than that of the healthy volunteer white matter for both radioligands. Uptake for individual WML in patients was heterogeneous, but the median WML DVR and NAWM DVR for individual patients were strongly correlated ($\rho = 0.94$, $P = 4 \times 10^{-11}$). A higher proportion of lesions were inactive in patients with SPMS (35%) than RRMS (23%), but active lesions were found in all patients, including those on highly efficacious treatments. **Conclusion:** TSPO radioligand uptake was increased in the brains of MS patients relative to healthy controls with 2 TSPO radiotracers. WML showed heterogeneous patterns of uptake. Active lesions were found in patients with both RRMS and SPMS. Their independent prognostic significance needs further investigation.

Key Words: multiple sclerosis; white matter lesions; TSPO; PET; microglia

J Nucl Med 2017; 58:1477–1482
DOI: 10.2967/jnumed.116.187161

Multiple sclerosis (MS) is a chronic disease of the central nervous system characterized by multifocal inflammatory demyelinating lesions. The number and distribution of the T2-hyperintense lesions (white matter lesions [WMLs]) in white matter found with MRI have a central role in the diagnosis of MS, but explain little of the future risk of disability progression (*1,2*).

The low predictive significance of WML may partially be explained by more diffuse inflammatory neuropathology evident in the white matter postmortem that appears normal on conventional MRI (*3*). Individual WML in the same brain and at different stages of disease also can have different neuropathologic characteristics not well distinguished by MRI (*4*). Innate immune responses involving proinflammatory microglia are associated with both the focal and the diffuse inflammation (*5–8*).

The 18-kDa mitochondrial translocator protein (TSPO) is highly expressed in activated microglia (*9*). Clinical studies using the first-generation TSPO PET radioligand ^{11}C-PK11195 reported higher global brain uptake in MS than healthy volunteers (HVs) (*10*). WML showed variably increased or decreased TSPO radioligand uptake (*11,12*). Recent studies have highlighted more diffuse uptake (*13,14*). However, a challenge to interpretation of the literature overall is the use of different radioligands and different analytic methods.

In the present study, we have assessed in vivo PET TSPO radioligand binding in MS patients with ^{11}C-PBR28 and reanalyzed previously published data obtained with ^{18}F-PBR111 (*13*) and in HVs with ^{11}C-PBR28 (*15–17*) using identical methodology. This allowed us to assess the consistency of results obtained with different radioligands and to compare characteristics of regional TSPO radioligand binding as an index of microglial/macrophage inflammatory activity in the MS normal-appearing white matter (NAWM) and within WML. We explored whether individual lesions could be distinguished by patterns of TSPO ligand binding in ways analogous to histopathologic classifications of lesions based on the distribution and abundance of activated microglia/macrophages (*18*).

MATERIALS AND METHODS

Subjects

The study protocol was approved by the West Bromley Research Ethics Committee (reference no. 14/LO/0445). All subjects signed a written informed consent form. MS was diagnosed according to the revised McDonald criteria (2010) (*19*). Subjects had an Expanded Disability Status Scale (EDSS) score of 7.0 or less, and none was treated with steroids or had a clinical relapse within 3 mo of scanning. MS patients and HVs scanned with ^{18}F-PBR111 and HVs scanned with ^{11}C-PBR28 were described previously (*13,15,17*).

Received Nov. 14, 2016; revision accepted Feb. 28, 2017.
For correspondence or reprints contact: Paul M. Matthews, E515, Division of Brain Sciences, Department of Medicine, Hammersmith Hospital, Du Cane Rd., London WC12 0NN, U.K.
E-mail: p.matthews@imperial.ac.uk
Published online Mar. 16, 2017.

TSPO Genotyping. TSPO genotype was assessed using a TaqMan-based polymerase chain reaction (Applied Biosystems; QuantStudio 7) assay specific for the rs6971 polymorphism in the TSPO gene (*20*). Participants having genotypes associated with low-affinity binding were excluded (*20,21*).

Imaging Methods

MR Scanning. MRI scans were obtained on a 3 T Trio scanner (^{11}C-PBR28 cohort) or a 3 T Verio scanner (^{11}C-PBR28 cohort) (both from Siemens Healthcare). Volumetric T1-weighted images were acquired for all subjects using a 1-mm isotropic resolution, before and 5 min after intravenous gadolinium chelate (Dotarem; Guerbet Laboratories Ltd.) administration. Volumetric T2-weighted images were acquired using a 1-mm isotropic resolution.

MR Image Processing and Definition of Regions of Interest. WMLs were segmented on the T2 image using Jim (Xinapse Systems, version 7). The WML mask was used for lesion-filling the T1 image before segmentation into white matter, gray matter, and cerebrospinal fluid with FMRIB Software Library tools (*22*). Perilesional masks were generated by dilating the WML mask in 3 dimensions by 6 mm and subtracting the WML mask. A NAWM mask was created by subtracting the dilated WML mask from the total white matter mask and eroding by 3 mm. The Clinical Imaging Centre Neuroanatomical Atlas was nonlinearly deformed into each individual's T1 brain space for anatomic parcellations of regions of interest for PET analyses (*23*).

PET Scanning and Radioligand Synthesis. PET scanning (Discovery RX PET/CT scanner; Siemens Healthcare Ltd.) was performed with a transaxial resolution of 5.0 mm and a radial resolution of 5.1 mm. ^{11}C-PBR28 or ^{18}F-PBR111 was injected as an intravenous bolus over approximately 20 s at the start of 90- and 120-min dynamic PET acquisitions, respectively (*15,21*).

Radiosynthesis and quality control were performed on site also as previously described, with radiochemical purities of greater than 95% (*15,21*).

PET Image and Kinetic Analysis. T1 images, NAWM, WML, caudate, and thalamus masks and reconstructed dynamic PET scans were used as inputs for the Molecular Imaging and Kinetic Analysis Toolbox software (www.miakat.org) for kinetic analysis of PET data. PET images were motion-corrected using SPM5 (Wellcome Trust Centre for Neuroimaging, http://www.fil.ion.ucl.ac.uk/spm) for frame-by-frame rigid realignment. SUVs were calculated from the time–activity curves between 60 and 90 min for ^{11}C-PBR28 and 90 and 120 min for ^{18}F-PBR111 (*15,21*). Transformed 4-dimensional PET images were integrated over time to obtain 3-dimensional PET summation images in Montreal Neurologic Institute 2-mm space (*23*).

Reference-based PET analyses enhance patient tolerance because arterial blood sampling is not needed. Here, we used the Logan graphical reference method (*24*) to estimate regional brain DVR using the caudate time–activity curve as the reference tissue input (*25*). Most previous MS studies also have used reference-based methods (*10–12,14,26–28*). We and others have confirmed that reference-based methods are strongly correlated with direct estimates of volume of distribution, V_T (*13,26,27,29*). However, the reference tissue ideally does not show specific (displaceable) ligand TSPO, which is expressed ubiquitously in the brain (*29*). Reference methods for TSPO have differed by the choice of reference tissue, broadly distinguished by those that use an individually variable reference, defined on the basis of appearing most similar to the behavior expected for the healthy brain (*26,27*) and those that are anatomically defined and selected identical for all subjects (*12,28*). We chose to use the latter, because the interpretation and assumptions of lack of interpatient heterogeneity are more directly tested.

All of these approaches technically define a pseudoreference region and vary in dynamic range or sensitivity by the extent and variance in radioligand uptake in the region selected. We used the caudate nucleus because it can be defined reliably using automated segmentation methods and shows relatively lower levels of microglial activation in MS patients and TSPO binding relative to other brain regions (*21*). We confirmed that there were no significant differences in the caudate SUV between people with MS and the HVs for ^{18}F-PBR111 (0.40 ± 0.11 for MS, 0.38 ± 0.07 for HVs, $P = 0.67$) and similarly for caudate SUV for ^{11}C-PBR28 (0.60 ± 0.14 for MS, 0.66 ± 0.13 for HV, $P = 0.26$). We directly tested the accuracy of the relative uptake estimated from the DVR calculated with the caudate pseudoreference region, and the ratio of SUV in brain regions to the SUV in caudate was strongly correlated with the DVR measure for MS and HVs for both radioligands (Supplemental Fig. 1; supplemental materials are available at http://jnm.snmjournals.org).

Individual Lesion Analysis and Classification

For the final analysis, WMLs with volume greater than 8 mm^3 were sampled to match the full width at half maximum of the PET scanner of approximately 5 mm. On the basis of earlier results (*30*) and new test–retest PET data (Supplemental Fig. 2), 4 classes of lesions were identified based on the presence of differences in DVR greater than 5% in the lesion core and in the perilesional volume relative to surrounding NAWM: high uptake relative to surrounding NAWM (active lesions), highest uptake in the perilesional volume (peripherally active lesions), uptake similar to the NAWM (undifferentiated lesions), and low uptake (inactive lesions).

Statistical Analysis

Statistical analyses were performed using SPSS software (SPSS version 22; IBM). The 1-way ANOVA was used to analyze the variance of between-subject factors. Homogeneity of variance was confirmed with the Levene test of equal variances. Post hoc analysis to assess differences between group means was performed, with correction for multiple comparisons (Tukey honest significant difference). Descriptive statistics were reported as mean ± SD, unless otherwise stated. For correlational analyses, the Spearman correlation coefficient was calculated, unless otherwise stated. A P value (Bonferroni-corrected for multiple comparisons) of less than 0.05 was considered statistically significant.

RESULTS

Demographic and clinical characteristics of study participants are summarized in Supplemental Tables 1 and 2. Data from 24 MS patients and 20 HVs scanned with ^{11}C-PBR28 and from 10 MS patients and 10 HVs scanned with ^{18}F-PBR111 are included. The MS patients studied with the 2 radioligands were well matched for age, sex, EDSS, and disease duration. However, approximately 30% of the ^{11}C-PBR28 PET cohort had SPMS, whereas all of those in the ^{18}F-PBR111 PET group had RRMS.

Brain TSPO Radioligand Uptake

There were significant differences in the ^{11}C-PBR28 DVR across brain regions for the MS and HVs (1-way ANOVA, $P = 4 \times 10^{-19}$). Uptake was highest in the thalamus; the thalamic ^{11}C-PBR28 DVR in patients with MS (1.52 ± 0.04) was higher than in HVs (1.39 ± 0.05, $P = 0.03$). The DVR of NAWM (1.17 ± 0.04) in the MS patients also was higher than in the white matter of HVs (1.02 ± 0.05, $P = 0.02$; Fig. 1A). ^{11}C-PBR28 uptake in the NAWM was greater for patients than the mean uptake across WML (1.03 ± 0.04, $P = 0.03$).

Our reanalysis of the smaller ^{18}F-PBR111 dataset found similar trends. Differences in DVR again were found between the MS and HV groups ($P = 1 \times 10^{-6}$). ^{18}F-PBR111DVR in the NAWM of the MS patients (1.27 ± 0.04) was greater than that in the HV white matter (1.13 ± 0.04, $P = 0.02$; Fig. 1B). The mean thalamic DVR

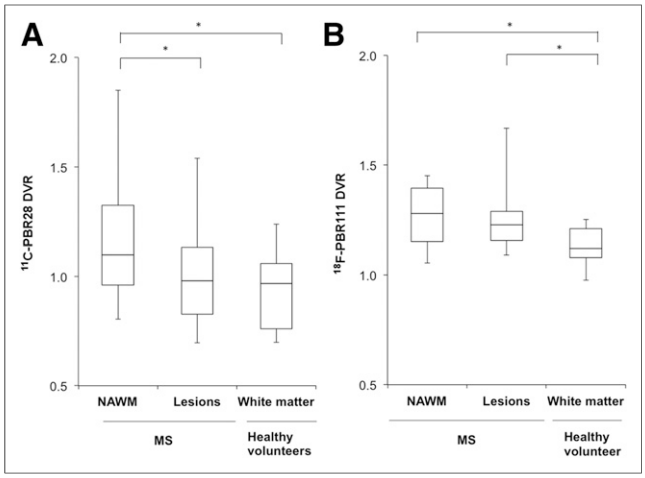

FIGURE 1. Box plots of DVR in white matter of HVs and NAWM and lesions in MS using ^{11}C-PBR28 (A) and ^{18}F-PBR111 (B). *$P < 0.05$ was considered a statistically significant different DVR between brain regions.

for MS patients (1.50 ± 0.04) was greater than for HVs (1.41 ± 0.04), although not statistically significantly ($P = 0.08$). We did not find differences between the mean DVR in the NAWM and WML ($P = 0.93$).

Baseline disability (EDSS) was not correlated with DVR in any brain region studied for either radioligand.

TSPO Binding in NAWM and Individual WML of MS Patients

We evaluated differences in white matter DVR between subjects (Fig. 2). The ranges in DVR for ^{11}C-PBR28 (median, 1.10; range, 0.80–1.85; Supplemental Fig. 3) and for ^{18}F-PBR111 (median, 1.28; range, 1.06–1.45) among MS patients both were greater than for the white matter of HVs (^{11}C-PBR28: median, 1.04, and range, 0.82–1.21; ^{18}F-PBR111: median, 1.12, and range, 0.98–1.25). Individual lesions in all subjects also showed a wide variation in DVR (Fig. 2). There was a strong correlation between the median WML DVR and NAWM DVR (Spearman $\rho = 0.94$ for both radioligands; $P = 4 \times 10^{-11}$ [^{11}C-PBR28] or $P = 1 \times 10^{-4}$ [^{18}F-PBR111]) (Fig. 3).

We found only 2 gadolinium-enhancing lesions in scans from the MS patients. The gadolinium-enhancing lesions (1 in a patient scanned with ^{11}C-PBR28 and 1 with ^{18}F-PBR111) had high DVR (1.81 and 1.19, respectively), but not the highest DVR of lesions within those subjects (Fig. 2, A22 and B3).

Classification of Individual Lesions Based on Relative TSPO Uptake

We pooled data from the ^{11}C-PBR28 and ^{18}F-PBR111 cohorts after classification of WML on the basis of the magnitude and spatial distribution of the relative TSPO ligand uptake as active, inactive, peripherally active, or undifferentiated ("Materials and Methods" section; Fig. 4). A higher proportion of lesions were inactive in patients with SPMS (35%, 39/112) than in those with RRMS (23%, 103/446, $P = 0.01$) (Fig. 5A). Inactive lesions were more common (31%, 39/126) in patients with a longer disease duration than in those with shorter disease duration (18%, 26/145, $P = 0.036$) (Fig. 5B). However, active lesions were found in both clinical stages of disease (RRMS: 18%, 82/446; SPMS: 28%, 31/112), across all quartiles of disease duration and in patients receiving any of the treatments represented in our population, as well as those not being treated (Fig. 5). Twenty-one percent (28/131) of sampled lesions in people being treated with nataluzimab (treated between 1 and 5.5 y) and 35% (24/69) of the lesions in those who had received alemtuzimab were classified as active. Undifferentiated lesions were relatively most common in the patients with RRMS who were treatment naïve (70%, 70/100).

DISCUSSION

We found similar relative differences between MS patients and HVs using both TSPO PET radioligands. Both were associated with heterogeneity of TSPO tracer uptake in NAWM and between lesions in the MS patients. The strong correlation between the NAWM and WML TSPO uptake for individual patients suggests that these measures both reflect the same individually variable, innate inflammatory phenotype. The differences in inflammatory activity were not well reflected in the conventional MRI measures; gadolinium enhancement identified only 2 lesions of a total of 558 lesions with increased TSPO radioligand uptake (Fig. 2). We found that lesions with diffusely high TSPO radioligand uptake (which we have called active lesions) can be found in all disease stages and treatment groups.

Although activated astrocytes can contribute to increased TSPO binding in some diseases, postmortem neuropathology suggests that activated microglia rather than astrocytes likely account for most TSPO binding in MS (*9*). The potential confound to quantitative estimation of the uptake of second-generation TSPO ligand differences in second-generation TSPO ligand affinity arising from the rs 6971 polymorphism can be addressed by genetic stratification (*20*).

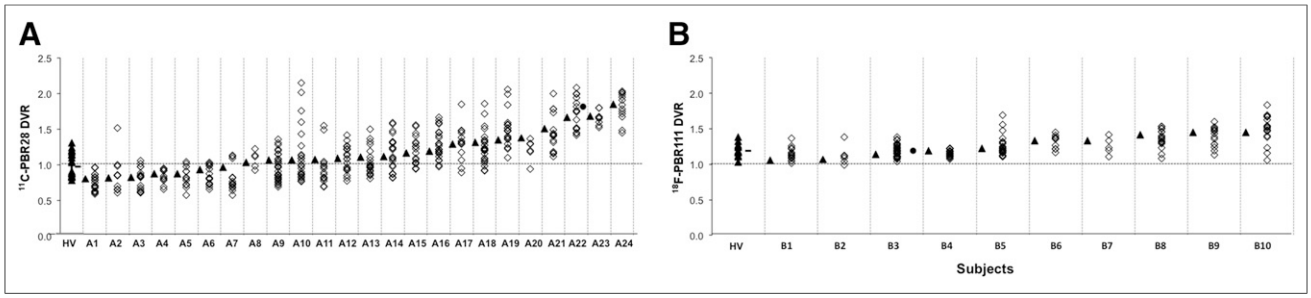

FIGURE 2. PET DVRs determined for ^{11}C-PBR28 (A) and ^{18}F-PBR111 (B) in white matter of individual HVs (▲ in HV column) and in NAWM (▲ in columns A1–A24 and B1–B10) and in individual WMLs (◇; median, horizontal black bar), including gadolinium-enhancing lesions (●) of MS patients. Data from all HVs are shown in single bar on far left side. Data from individual MS patients (rank ordered with respect to NAWM DVR) are shown to right. A1–A24 and B1–B10 denote individual MS patients scanned with ^{11}C-PBR28 and ^{18}F-PBR111, respectively. Detailed demographic information is provided in Supplemental Table 2.

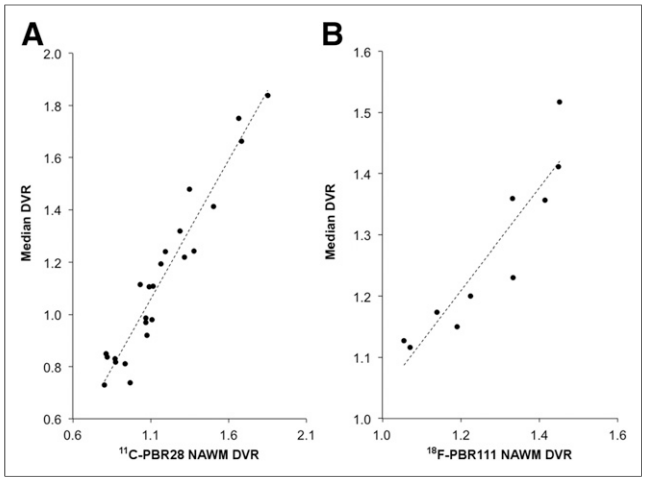

FIGURE 3. Strong positive correlations between median PET DVRs were found using both ^{11}C-PBR28 (A) (Spearman $\rho = 0.94$, $P = 4 \times 10^{-11}$) and ^{18}F-PBR111 (B) ($\rho = 0.94$, $P = 1 \times 10^{-4}$) between DVR in WMLs (ordinate) and in NAWM (abscissa) for MS patients.

Interpretation of differences in binding in terms of microglial activation in MS can thus be done with some confidence.

Neuropathology studies and in vivo PET TSPO imaging both provide evidence for a diffuse inflammatory process in white matter. This is associated with evidence of neuronal injury (*18,31,32*). Focal clusters or nodules of white matter microglial activation may precede the formation of WML (*33*). Consistent with these observations (and prior studies using ^{11}C-PK11195), we found that TSPO binding was higher in the NAWM than in the white matter of HVs (*11,12,14*). Increased uptake in the NAWM of patients with clinically isolated syndrome is associated with early development of clinically definite MS (*34*).

We found a heterogeneous pattern of microglial activation in WML relative to the NAWM both between and within MS patients. This heterogeneity is consistent with postmortem histopathology, which shows variable microglial activation between lesions (*6,35*). Prior studies also have shown variable TSPO radioligand uptake within lesions relative to NAWM (*11,12*). What has not been noted before is the strong correlation between the TSPO binding in NAWM and in WML. This suggests that patients are better described in terms of a global inflammatory state of their white matter rather than by individual lesion activity. Extending the earlier observations with clinically isolated syndrome (*34*), measures of this global white matter innate inflammatory activity may be predictive of the short-term disease course generally for patients with MS.

We classified individual lesions into 4 different classes based on the patterns of TSPO radioligand uptake relative to that in the surrounding NAWM. The classification is similar conceptually to that used histopathologically for WML in MS brains: both rely on differences in distributions of activated microglia (*35*). In our study, we identified all 4 of these lesion types in vivo in all disease stages. There was a higher proportion of inactive lesions in patients with longer disease duration and with SPMS than with RRMS. These findings in vivo are reflected in a recent study of brains postmortem, in which histopathologically defined inactive lesions are more common with SPMS and longer disease duration (*5*). However, we also found that TSPO PET active lesions were more common in brains of patients with SPMS than in those from patients with RRMS. Unexpectedly, we found active lesions even in patients receiving either of 2 of the most efficacious pharmacologic immunomodulators (alemtuzimab and nataluzimab).

These data thus provide further evidence for substantial persistent innate inflammatory activity in SPMS (*10*). They also suggest that current treatments classed as highly efficacious based on suppression of T2 hyperintense lesion activity do not suppress microglial activity fully. Persistent, proinflammatory microglia could explain the progression of neurodegenerative changes reflected as brain atrophy or disability progression that are seen in some patients (*35*). However, alternative microglial activation phenotypes also can contribute to reparative processes (*36*).

Baseline T2 lesion load and clinical progression are weakly correlated (*37*). Previous TSPO PET studies have reported positive correlations between disability (EDSS) and TSPO ligand uptake (*10,13*), but we did not observe this with either of our 2 patient groups. This may be related to sample sizes, as neither study was powered for this outcome. The lack of correlation between disability and TSPO uptake could reflect limitations of a cross-sectional design: disability measures reflect the summary impact of relevant injury to date, whereas the PET measures are determined by inflammatory activity only at the time of the scan. Insensitivity of EDSS to all relevant dimensions of disability could also contribute (*38*). Finally, quantifying TSPO binding using a pseudoreference region method may have led to an underestimation of regional radioligand uptake (35). The reduced dynamic range of the reference-based measure could limit discrimination of differences between tissues, despite the gain in precision. We also did not have repeated examinations on all subjects, so we had to define meaningful differences in DVR based on a hard threshold estimated from independent test–retest estimates.

In vitro, ex vivo, and in silico data indicate that ^{11}C-PBR28 has a higher binding affinity for TSPO and higher displaceable-to-nondisplaceable binding than ^{18}F-PBR111, when matched for

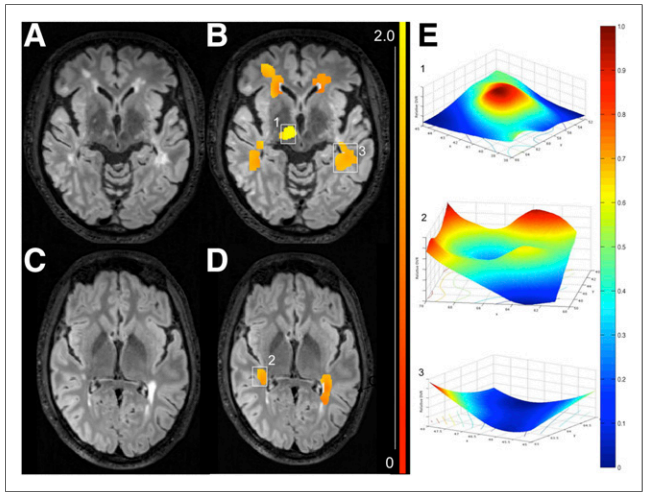

FIGURE 4. Axial T2 fluid-attenuated inversion recovery MR images (A–D) from 2 MS patients (participants A20 [A and B] and A10 [C and D], respectively) with corresponding overlays of parametric ^{11}C-PBR28 PET DVRs within and around larger white matter T2 hyperintense lesions (B and D). To their right is a color scale for DVR values. (E) Includes surface renderings of relative DVR variation across voxels for lesions identified as to the left as 1–3 (B and D). To discriminate voxelwise variation more clearly, DVR has been transformed by a nonlinear scaling function, with relative values expressed as shown on color scale to right and as relative excursion above origin. The base of plot has axes ordered by voxels in image plane (*x, y*). Three lesion types are illustrated: (1) an active lesion, (2) a peripherally active lesion, and (3) an undifferentiated lesion.

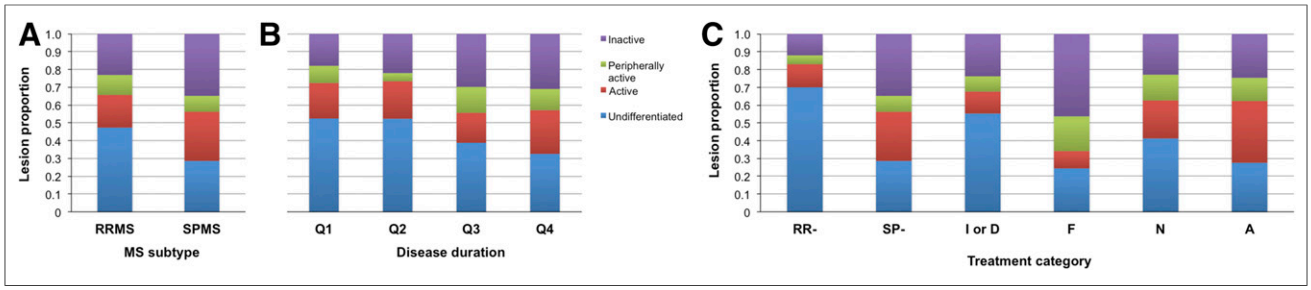

FIGURE 5. Proportions of the 4 types of WMLs characterized by PET in MS patients. Data from subjects studied with ^{11}C-PBR28 and ^{18}F-PBR111 have been combined. Plots illustrate relative abundance of lesions classified by clinical MS subtype (relapsing remitting [RR], secondary progressive [SP]) (A) and disease duration of subjects (expressed as quartiles [Q] across the study population: Q1, 1–7 y; Q2, 8–11 y; Q3, 12–16 y; Q4, 17–28 y) (B). (C) Relative proportion of lesion group according to treatment at time of scanning: no treatment in people with relapsing remitting (RR-) or secondary progressive (SP-); disease-modifying treatment with interferon or dimethyl fumarate (I or D), fingolimod (F), nataluzimab (N), and alemtuzimab (A).

TSPO binding status (*39*). A study using a TSPO agonist (XBD173) to block binding of ^{11}C-PBR28 in HVs directly confirmed estimates of relatively high displaceable (specific) binding for this ligand (*15*). The dynamic range of DVR in the MS patients measured with ^{11}C-PBR28 was greater than with ^{18}F-PBR111. Finally, defluorination of the ^{18}F-PBR111 and skull uptake of ^{18}F (*40*) limit accuracy of assessment of uptake in the adjacent neocortex. Together, these factors suggest that for many applications, ^{11}C-PBR28 is a preferable radioligand. However, the longer half-life of ^{18}F-PBR111 (110 min) than ^{11}C-PBR28 (20 min) makes the former more practical for transportation between sites without the need for having an on-site cyclotron to produce the radioligand. Further work needs to be done, for instance, with blocking studies of ^{18}F-PBR111, to characterize the in vivo binding characteristics of both radioligands, but depending on manufacturer/supply arrangements ^{18}F-PBR111 could have advantages at some sites.

CONCLUSION

Our report provides further evidence for continuing inflammation and heterogeneity in the innate immune inflammatory activity of individual lesions and NAWM of patients with MS that is not captured by conventional MRI. Our results highlight that gadolinium contrast enhancement underestimates the total inflammatory activity. We also found that the overall innate inflammatory activity was not appreciably lower in patients with RRMS relative to SPMS. We hypothesize that this inflammation contributes to determining the prognosis of individual patients. PET may provide a pharmacodynamic marker for treatments targeting this activity. Longitudinal studies now are needed to establish the clinical significance of these and related observations from other laboratories.

DISCLOSURE

Paul M. Matthews, Anne Lingford-Hughes, Alessandro Colasanti, Nicola Kalk, and Gourab Datta received support from grants from GSK during the conduct of these studies. Eugenii A. Rabiner and Paul M. Matthews are past employees and current shareholders in GSK. No other potential conflict of interest relevant to this article was reported.

ACKNOWLEDGMENTS

Gourab Datta is grateful for support as a fellow through the Imperial Wellcome Trust-GlaxoSmithKline Clinical Fellowship Training Scheme. This article presents independent research funded by this fellowship scheme and supported by the NIHR CRF at Imperial College Healthcare NHS Trust. Paul M. Matthews acknowledges generous support from the Edmond J Safra Foundation and Lily Safra and research funding through the Imperial Biomedical Research Centre and the NIHR Investigator programme.

REFERENCES

1. Bar-Zohar D, Agosta F, Goldstaub D, Filippi M. Magnetic resonance imaging metrics and their correlation with clinical outcomes in multiple sclerosis: a review of the literature and future perspectives. *Mult Scler.* 2008;14:719–727.
2. Goodin DS. Magnetic resonance imaging as a surrogate outcome measure of disability in multiple sclerosis: have we been overly harsh in our assessment? *Ann Neurol.* 2006;59:597–605.
3. Allen IV, McQuaid S, Mirakhur M, Nevin G. Pathological abnormalities in the normal-appearing white matter in multiple sclerosis. *Neurol Sci.* 2001;22:141–144.
4. Filippi M, Rocca MA, Barkhof F, et al. Association between pathological and MRI findings in multiple sclerosis. *Lancet Neurol.* 2012;11:349–360.
5. Frischer JM, Weigand SD, Guo Y, et al. Clinical and pathological insights into the dynamic nature of the white matter multiple sclerosis plaque. *Ann Neurol.* 2015;78:710–721.
6. Frischer JM, Bramow S, Dal-Bianco A, et al. The relation between inflammation and neurodegeneration in multiple sclerosis brains. *Brain.* 2009;132:1175–1189.
7. Mahad DH, Trapp BD, Lassmann H. Pathological mechanisms in progressive multiple sclerosis. *Lancet Neurol.* 2015;14:183–193.
8. Kutzelnigg A, Lucchinetti CF, Stadelmann C, et al. Cortical demyelination and diffuse white matter injury in multiple sclerosis. *Brain.* 2005;128:2705–2712.
9. Cosenza-Nashat M, Zhao ML, Suh HS, et al. Expression of the translocator protein of 18 kDa by microglia, macrophages and astrocytes based on immunohistochemical localization in abnormal human brain. *Neuropathol Appl Neurobiol.* 2009;35:306–328.
10. Politis M, Giannetti P, Su P, et al. Increased PK11195 PET binding in the cortex of patients with MS correlates with disability. *Neurology.* 2012;79:523–530.
11. Banati RB, Newcombe J, Gunn RN, et al. The peripheral benzodiazepine binding site in the brain in multiple sclerosis: quantitative in vivo imaging of microglia as a measure of disease activity. *Brain.* 2000;123:2321–2337.
12. Debruyne JC, Versijpt J, Van Laere KJ, et al. PET visualization of microglia in multiple sclerosis patients using [^{11}C]PK11195. *Eur J Neurol.* 2003;10:257–264.
13. Colasanti A, Guo Q, Muhlert N, et al. In vivo assessment of brain white matter inflammation in multiple sclerosis with ^{18}F-PBR111 PET. *J Nucl Med.* 2014;55:1112–1118.
14. Rissanen E, Tuisku J, Rokka J, et al. In vivo detection of diffuse inflammation in secondary progressive multiple sclerosis using PET imaging and the radioligand ^{11}C-PK11195. *J Nucl Med.* 2014;55:939–944.
15. Owen DR, Guo Q, Kalk NJ, et al. Determination of [^{11}C]PBR28 binding potential in vivo: a first human TSPO blocking study. *J Cereb Blood Flow Metab.* 2014;34:989–994.
16. Vera JH, Guo Q, Cole JH, et al. Neuroinflammation in treated HIV-positive individuals: a TSPO PET study. *Neurology.* 2016;86:1425–1432.

17. Guo Q, Owen DR, Rabiner EA, Turkheimer FE, Gunn RN. A graphical method to compare the in vivo binding potential of PET radioligands in the absence of a reference region: application to [^{11}C]PBR28 and [^{18}F]PBR111 for TSPO imaging. *J Cereb Blood Flow Metab.* 2014;34:1162–1168.
18. Lassmann H, Bruck W, Lucchinetti CF. The immunopathology of multiple sclerosis: an overview. *Brain Pathol.* 2007;17:210–218.
19. Polman CH, Reingold SC, Banwell B, et al. Diagnostic criteria for multiple sclerosis: 2010 revisions to the McDonald criteria. *Ann Neurol.* 2011;69:292–302.
20. Owen DR, Yeo AJ, Gunn RN, et al. An 18-kDa translocator protein (TSPO) polymorphism explains differences in binding affinity of the PET radioligand PBR28. *J Cereb Blood Flow Metab.* 2012;32:1–5.
21. Guo Q, Colasanti A, Owen DR, et al. Quantification of the specific translocator protein signal of ^{18}F-PBR111 in healthy humans: a genetic polymorphism effect on in vivo binding. *J Nucl Med.* 2013;54:1915–1923.
22. Battaglini M, Jenkinson M, De Stefano N. Evaluating and reducing the impact of white matter lesions on brain volume measurements. *Hum Brain Mapp.* 2012;33:2062–2071.
23. Tziortzi AC, Searle GE, Tzimopoulou S, et al. Imaging dopamine receptors in humans with [^{11}C]-(+)-PHNO: dissection of D3 signal and anatomy. *Neuroimage.* 2011;54:264–277.
24. Logan J, Fowler JS, Volkow ND, Wang GJ, Ding YS, Alexoff DL. Distribution volume ratios without blood sampling from graphical analysis of PET data. *J Cereb Blood Flow Metab.* 1996;16:834–840.
25. Gunn RN, Gunn SR, Cunningham VJ. Positron emission tomography compartmental models. *J Cereb Blood Flow Metab.* 2001;21:635–652.
26. Turkheimer FE, Edison P, Pavese N, et al. Reference and target region modeling of [^{11}C]-(R)-PK11195 brain studies. *J Nucl Med.* 2007;48:158–167.
27. Herranz E, Gianni C, Louapre C, et al. Neuroinflammatory component of gray matter pathology in multiple sclerosis. *Ann Neurol.* 2016;80:776–790.
28. Colasanti A, Guo Q, Giannetti P, et al. Hippocampal neuroinflammation, functional connectivity, and depressive symptoms in multiple sclerosis. *Biol Psychiatry.* 2016;80:62–72.
29. Kropholler MA, Boellaard R, Schuitemaker A, Folkersma H, van Berckel BN, Lammertsma AA. Evaluation of reference tissue models for the analysis of [^{11}C](R)-PK11195 studies. *J Cereb Blood Flow Metab.* 2006;26:1431–1441.
30. Coughlin JM, Wang Y, Ma S, et al. Regional brain distribution of translocator protein using [^{11}C]DPA-713 PET in individuals infected with HIV. *J Neurovirol.* 2014;20:219–232.
31. Geurts JJ, Bo L, Roosendaal SD, et al. Extensive hippocampal demyelination in multiple sclerosis. *J Neuropathol Exp Neurol.* 2007;66:819–827.
32. Lassmann H, van Horssen J, Mahad D. Progressive multiple sclerosis: pathology and pathogenesis. *Nat Rev Neurol.* 2012;8:647–656.
33. Singh S, Metz I, Amor S, van der Valk P, Stadelmann C, Bruck W. Microglial nodules in early multiple sclerosis white matter are associated with degenerating axons. *Acta Neuropathol (Berl).* 2013;125:595–608.
34. Giannetti P, Politis M, Su P, et al. Increased PK11195-PET binding in normal-appearing white matter in clinically isolated syndrome. *Brain.* 2015;138:110–119.
35. Lucchinetti C, Bruck W, Parisi J, Scheithauer B, Rodriguez M, Lassmann H. Heterogeneity of multiple sclerosis lesions: implications for the pathogenesis of demyelination. *Ann Neurol.* 2000;47:707–717.
36. Ransohoff RM. A polarizing question: do M1 and M2 microglia exist? *Nat Neurosci.* 2016;19:987–991.
37. Sormani MP, Arnold DL, De Stefano N. Treatment effect on brain atrophy correlates with treatment effect on disability in multiple sclerosis. *Ann Neurol.* 2014;75:43–49.
38. Stangel M, Penner IK, Kallmann BA, Lukas C, Kieseier BC. Towards the implementation of 'no evidence of disease activity' in multiple sclerosis treatment: the multiple sclerosis decision model. *Ther Adv Neurol Disord.* 2015;8:3–13.
39. Guo Q, Owen DR, Rabiner EA, Turkheimer FE, Gunn RN. Identifying improved TSPO PET imaging probes through biomathematics: the impact of multiple TSPO binding sites in vivo. *Neuroimage.* 2012;60:902–910.
40. Fookes CJ, Pham TQ, Mattner F, et al. Synthesis and biological evaluation of substituted [^{18}F]imidazo[1,2-a]pyridines and [^{18}F]pyrazolo[1,5-a]pyrimidines for the study of the peripheral benzodiazepine receptor using positron emission tomography. *J Med Chem.* 2008;51:3700–3712.